Ferroelectric and ferrimagnetic iron-doped thin-film $BaTiO_3$: Influence of iron on physical properties

R. Maier and J. L. Cohn[a)]
Department of Physics, University of Miami, Coral Gables, Florida 33124

(Received 14 December 2001; accepted 3 August 2002)

Structural and physical properties of ferroelectric and ferrimagnetic pulsed-laser deposition-grown thin-film $BaFe_xTi_{1-x}O_3$ with $0.5 \leqslant x \leqslant 0.75$ (BFTO) are compared with those of $BaTiO_3$ (BTO) films deposited under identical conditions. Fe leads to lattice expansion and deterioration of the crystalline quality in the as-prepared films. Signatures of the paraelectric–ferroelectric phase transition in lattice parameters, resistivity, and capacitance tend to be suppressed in BTO films, but are clearly distinguished in the presence of Fe. While strain elevates T_C above bulk values in thin-film BTO to ~200 °C, Fe doping entails further increases of T_C up to ~320 °C. Current versus voltage measurements demonstrate that Fe converts *n*-type BTO into *p*-type BFTO. Fe doping brings about ferrimagnetic ordering with a Néel temperature above 450 °C. © *2002 American Institute of Physics.* [DOI: 10.1063/1.1510591]

I. INTRODUCTION

Recently, we reported physical properties of a new metastable phase of thin-film iron-doped $BaTiO_3$ (BFTO) in which ferroelectricity and ferrimagnetism coexist.[1] Such materials are quite rare, particularly at room temperature and above, and offer the prospect of devices in which, for instance, the polarization or the transition temperature is manipulated via magneto- or electrostriction.

Whereas thin-film pseudocubic $BaFe_xTi_{1-x}O_3$ with $0.5 \leqslant x \leqslant 0.75$ has not been investigated before, much work has been done on thin-film $BaTiO_3$ (BTO) during the last decade. These efforts were mainly triggered by interest in improved materials for memory and optical applications. The physical properties of thin-film BTO differed substantially from those of bulk BTO: The dielectric constant was usually significantly lower,[2,3] hysteresis loops were often absent,[4] and the nature of the ferroelectric–paraelectric phase transition was modified.[5,6]

The main motivation of the present article is to clarify the role of iron on the structural and physical properties of BFTO. For this purpose, thin-film BFTO is compared to thin-film BTO made under identical conditions, and BFTO films of three different iron concentrations are compared to each other. Particular attention is focused on the paraelectric–ferroelectric phase transition. We present data on the temperature dependence of lattice constants, electrical resistivity, current versus voltage ($I-V$), capacitance, and magnetization.

II. EXPERIMENT

Thin films were grown by pulsed-laser deposition (PLD) with a 248 nm KrF excimer laser (Lambda Physik, Compex 205) at 10–20 Hz pulse repetition rate, 4 cm target–substrate distance, and ~1.3–2.0 J/cm^2 energy density at the target. Three different BFTO targets, prepared by solid-state reaction,[7,8] were used: $BaTi_{0.5}Fe_{0.5}O_3$, $Ba_4Fe_4Ti_3O_{16}$ (BFTO-E), and $BaTi_{0.25}Fe_{0.75}O_3$. The BTO target was obtained from Superconductive Components, Inc. Both BFTO and BTO were deposited on [100]MgO and 0.05 wt % Nb-doped [100]$SrTiO_3$ (STON) substrates; BFTO films were also deposited on [110]MgO, [111]MgO, and [100]$SrTiO_3$ (STO). Substrate temperature during deposition was 880 °C. Oxygen pressure during deposition was $P_{O_2} = 100$ mTorr for all BFTO films; BTO films were deposited at both 100 mTorr and 0.12 mTorr. For films made at $P_{O_2} = 100$ mTorr, P_{O_2} was increased to 500 Torr following the depositions, and the films were cooled to 500 °C at 5 °C/min, held for 30 min, and then cooled to room temperature at natural rate. The BTO films deposited at $P_{O_2} = 0.12$ mTorr were kept at deposition pressure and cooled to room temperature at 10 °C/min. In this article, we adopt the notation "$BTO_{100mTorr}$" and "$BTO_{0.12mTorr}$" to distinguish between BTO films made at a different P_{O_2}. Also, we will write "BF50," "BFTE," and "BF75" for films made from the $BaTi_{0.5}Fe_{0.5}O_3$ target, the BFTO-E target, and the $BaTi_{0.25}Fe_{0.75}O_3$ target, respectively.

X-ray diffraction (XRD) was performed with a Philips X'Pert diffractometer equipped with a small heating stage that enabled XRD measurements at temperatures up to 300 °C. Film thicknesses were computed from the number of laser pulses, with calibrations at several thicknesses using transmission electron microscopy (TEM) cross-sectional images.[7] Thicknesses covered a broad range from 30 nm–8 μm for BFTO; all BTO films were ~360 nm thick.

Electrical properties were measured normal to plane in films deposited on metallic STON (bottom electrode) with thermally evaporated circular Au or Cr–Au overlayers of 1.5 mm diameter (top electrode). For brevity, we call these heterostructures "BTO capacitors," "BF50 capacitors" etc. In-plane electrical resistivity was measured in films deposited on [100]MgO using silver-paint electrodes. Electrical resistivity and $I-V$ were measured with a two-probe method us-

a)Electronic mail: cohn@physics.miami.edu

 © 2002 American Institute of Physics

Downloaded 26 Sep 2007 to 129.171.61.70. Redistribution subject to AIP license or copyright, see http://jap.aip.org/jap/copyright.jsp

ing a Keithley 6512 electrometer and a Keithley 230 voltage source. $I-V$ measurements used voltage steps of 0.1 V, maximum voltage ± 2.5 V, and ~ 1 s delay between steps. To eliminate shorting through the sample stage, some specimens were suspended from their leads and the latter supported by a long, thin plastic rod. Capacitance measurements were performed with a HP4263B LCR meter at frequencies $\leqslant 100$ kHz with 20 mV or 50 mV ac-voltage amplitude. $C-V$ measurements employed the Keithley 230 voltage source with voltage steps 0.1 V or 0.2 V; the time delay between steps was 5 min for a $BTO_{100mTorr}$ sample and ~ 30 s for a BF75 sample. Magnetization was measured with a Quantum Design magnetometer with field applied parallel to the film plane.

III. THIN-FILM MICROSTRUCTURE

A. X-ray data at room temperature

Electron microprobe analysis performed on BFTO indicated film compositions consistent with those of the targets.[7] Pseudocubic structure and epitaxial, cube-on-cube growth on all substrates was confirmed by XRD for both BFTO and BTO as described elsewhere.[7,9]

The actual structure of the as-prepared films is tetragonal or weakly orthorhombic, as confirmed by asymmetric rocking curve scans[10] of the {303} film reflections. The out-of-plane lattice parameter will be denoted $a_\perp$, the two in-plane lattice parameters $a_{\parallel 1}$ and $a_{\parallel 2}$. Two different orientations of the (tetragonal) unit cell relative to the film plane occur in the films: $a_\perp = a$ (a orientation) and $a_\perp = c$ (c orientation).

BFTO films have $a_\perp \cong 4.03-4.07$ Å, $a_\parallel \cong 4.04-4.08$ Å, and are a oriented with c/a-ratio smaller than that of bulk BTO ($c = 4.0336$ Å, $a = 3.9947$ Å at room temperature).[11] $BTO_{100mTorr}$ films have $a_\perp \cong 3.99-4.00$ Å and $a_\parallel \cong 4.01-4.03$ Å, and are a oriented with c/a ratio comparable to that of bulk BTO. $BTO_{0.12mTorr}$ films have $a_\perp \cong 4.08-4.10$ Å and $a_\parallel \cong 4.02-4.04$ Å, and are c oriented with c/a ratio comparable to that of bulk BTO.

The a-oriented films are usually slightly orthorhombic with the in-plane parameters $a_{\parallel 1}$, $a_{\parallel 2}$ closer to each other than to the out-of-plane parameter $a_\perp$. Presumably, the larger of $a_{\parallel 1}$, $a_{\parallel 2}$ corresponds to c in relaxed tetragonal BTO, whereas $a_\perp$ and the smaller parameter of $a_{\parallel 1}$, $a_{\parallel 2}$ correspond to a. That one of the original a parameters is closer to c than it is to the other a parameter is likely a consequence of in-plane stress.

Crystalline quality assessed from rocking curves of the (002) reflection was highest in $BTO_{100mTorr}$, lowest in BFTO, and generally higher on STO than on MgO. Figure 1 shows a rocking curve of the (200) reflection for $BTO_{100mTorr}$ on STO. The full width at half maximum (FWHM) is 0.195°, whereas it is 0.39° for $BTO_{100mTorr}$ on MgO. These values indicate a quality among the best achieved for BTO films with a thickness <500 nm on these substrates.[12,13] The superior quality achieved on STO ($a = 3.905$ Å)[14] as compared to MgO ($a = 4.213$ Å)[14] is attributed to smaller lattice mismatch on STO.

In $BTO_{0.12mTorr}$ the FWHM is 0.31° on STO and 0.51° on MgO. The inferior quality in $BTO_{0.12mTorr}$ as compared to $BTO_{100mTorr}$ is attributed to oxygen vacancies. In BFTO, rocking curves of the (002) peak yielded FWHMs of at least 0.6° for all compositions and substrates. Evidently, the Fe substitution further reduces the structural quality due to atomic disorder and/or associated changes in the grain morphology.

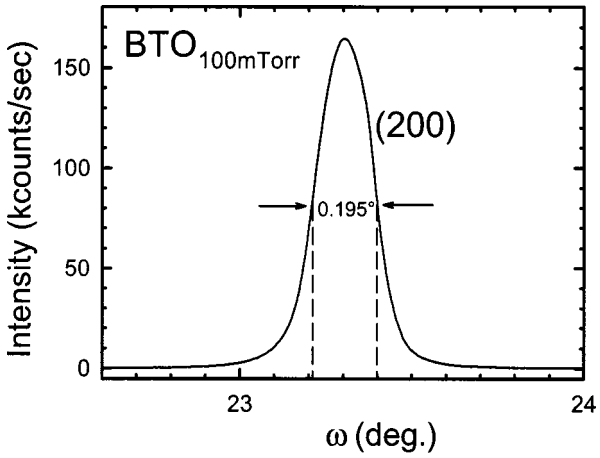

FIG. 1. X-ray θ-scan of the (200) reflection of a $BTO_{100mTorr}$ film.

In addition to the part of the pseudocubic phase that grows cube on cube with the substrate, several secondary orientations of the same phase exist in the films,[15] which have been previously reported for BTO films.[12,13,16] Distinct from the pseudocubic phase, TEM revealed a disordered phase in BFTO films;[7] it formed during the latter stages of deposition in only the thickest films (>1 μm).

In summary, BFTO (and BTO) films grow epitaxially on STO and MgO. In the as-prepared state, the main phase is a oriented and pseudocubic orthorhombic, except for $BTO_{0.12mTorr}$ (c oriented, pseudocubic tetragonal). The lattice parameters in BFTO are expanded as compared to $BTO_{100mTorr}$, and even more so in $BTO_{0.12mTorr}$. The crystalline quality as inferred from rocking curves is highest in $BTO_{100mTorr}$.

B. Unit-cell volume and orientation relative to the film plane

Oxygen vacancies, which expand the lattice in perovskites,[17,18] are the likely mechanism for the expanded lattices observed for BFTO and $BTO_{0.12mTorr}$ films. $BTO_{0.12mTorr}$ is oxygen deficient because of the low partial pressure of oxygen during deposition. The substitution of Fe in BTO implies[19] the oxidation of Fe^{3+} to Fe^{4+} and/or the formation of one oxygen vacancy for two Fe^{3+}. The larger[20] ionic radius of Fe^{3+} (0.645 Å, CN$=6$) as compared to Ti^{4+} (0.605 Å) may also contribute to the expansion in BFTO films.

The orientation of the unit cells relative to the film plane is determined by the in-plane stress just above T_C during cooling from the deposition temperature.[21] Tensile (compressive) in-plane stress favors $a(c)$ orientation.[21] Lattice expansion, thermal expansion mismatch[22] and thermal vibration[23,24] are the primary sources of this stress. For 100 mTorr deposition pressure, the contribution of the latter

Downloaded 26 Sep 2007 to 129.171.61.70. Redistribution subject to AIP license or copyright, see http://jap.aip.org/jap/copyright.jsp

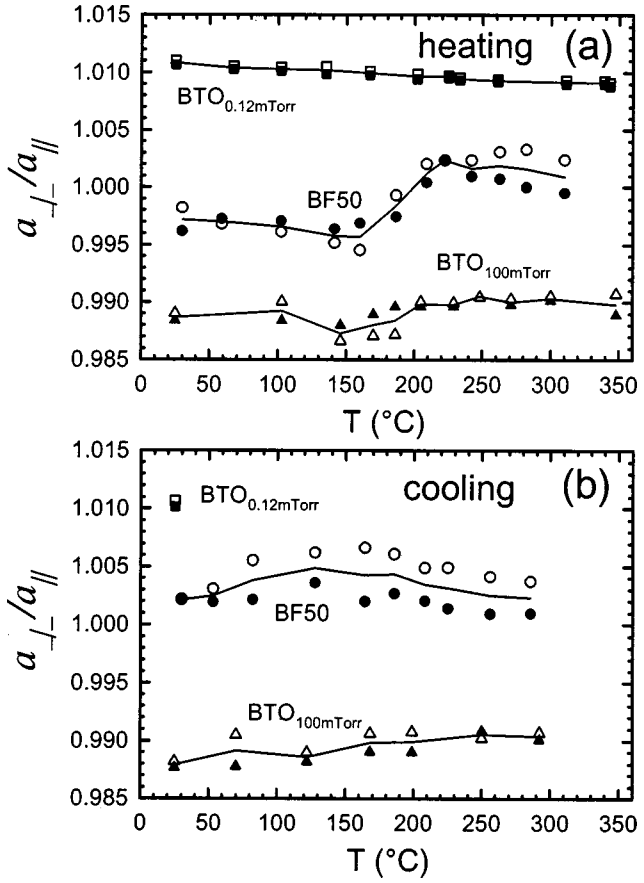

FIG. 2. Temperature evolution of lattice constants in BF50, $BTO_{100mTorr}$, and $BTO_{0.12mTorr}$. All three films are ~360 nm thick; BF50 was deposited on STO, the others on STON. Closed symbols denote $a_\perp/a_{\parallel 1}$, open symbols $a_\perp/a_{\parallel 2}$, and the solid curves $a_\perp/a_{\parallel avg}$.

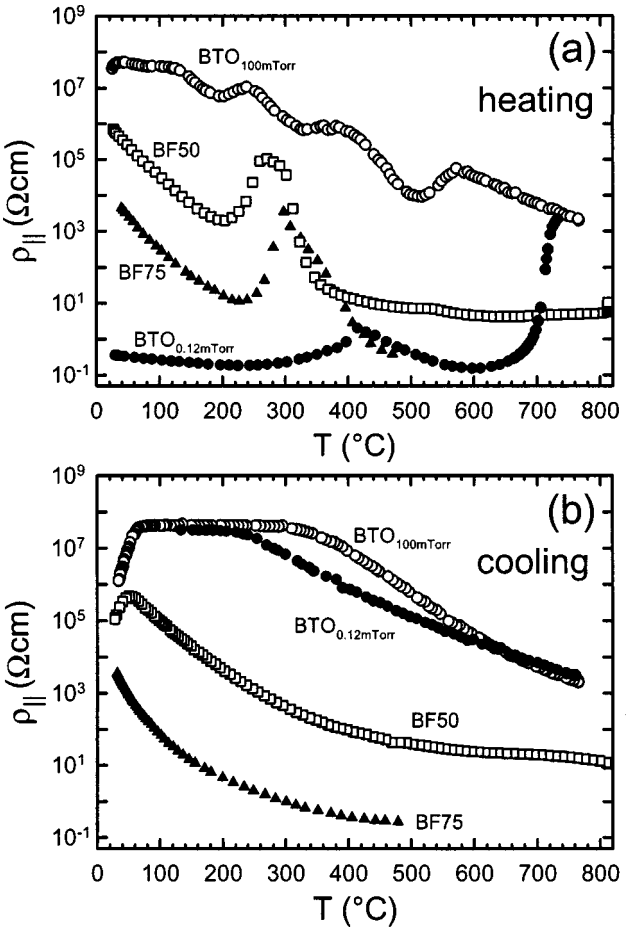

FIG. 3. In-plane resistivity vs temperature for as-prepared films from each of the four targets deposited on [100]MgO. BF50 is ~70 nm thick, the others are ~360 nm thick: (a) heating and (b) cooling.

mechanism is less significant than the other two, and the *a* orientation follows from a net in-plane tensile stress. At low pressure, the kinetic energy of the oncoming particles is much larger so that thermal vibration induces considerable compressive in-plane stress. This results in a *c* orientation for $BTO_{0.12mTorr}$ on both substrates.

C. X-ray data at elevated temperatures

Figure 2 shows the temperature evolution of the ratios $a_\perp/a_{\parallel 1}$ and $a_\perp/a_{\parallel 2}$ for $BTO_{0.12mTorr}$, $BTO_{100mTorr}$, and BF50, grown on STO or STON. The room-temperature data prior to heating reflect the structures and orientations described in Sec. III A for the as-prepared state. Upon heating [Fig. 2(a)], the BF50 film exhibits a structural transition from *a* oriented to *c* oriented (or cubic) between 180 °C and 220 °C. A substantially weaker structural anomaly is suggested by the data for $BTO_{100mTorr}$ in the range 150 °C–200 °C, but the average structure remains *a* oriented. $BTO_{0.12mTorr}$ shows no structural anomalies. Upon cooling to room temperature, the structures of the BTO films are very close to that of their as-prepared states. In contrast, the BF50 film shows thermal hysteresis; apparently, it remains in the *c*-oriented state to which it transformed during heating.

IV. THIN-FILM ELECTRICAL PROPERTIES

A. Resistivity and current–voltage curves

The in-plane resistivity $\rho_\parallel$ versus temperature is shown in Fig. 3 for films of all compositions. $\rho_\parallel$ is highest for $BTO_{100mTorr}$ at most temperatures and decreases as iron is added. $\rho_\parallel$ is lowest for $BTO_{0.12mTorr}$, in agreement with previous reports[25] of enhanced conductivity in BTO associated with oxygen vacancies (which act as shallow donors). The increased conductivity of BFTO can be attributed principally to oxygen vacancies induced by Fe doping. Fe^{3+} acceptor states in bulk BTO have expected ionization energies ~0.42 eV as compared with ~0.1 eV for oxygen-vacancy donors.[26] The normal-to-plane resistivities $\rho_\perp$ are several orders of magnitude higher than the corresponding in-plane resistivities,[15] likely due to barriers at the electrode interfaces.

A semiconducting behavior with $d\rho_\parallel/dT<0$ is generally observed upon heating [Fig. 3(a)], but there are temperature intervals where $d\rho_\parallel/dT>0$. Such positive-temperature coefficient of resistance (PTCR) anomalies,[27–29] typical of polycrystalline BTO and other ferroelectric ceramics, are associated with a potential barrier at grain-boundary Schottky contacts. This barrier is controlled by the high-field dielectric constant of the semiconducting grains; the decrease of the

Downloaded 26 Sep 2007 to 129.171.61.70. Redistribution subject to AIP license or copyright, see http://jap.aip.org/jap/copyright.jsp

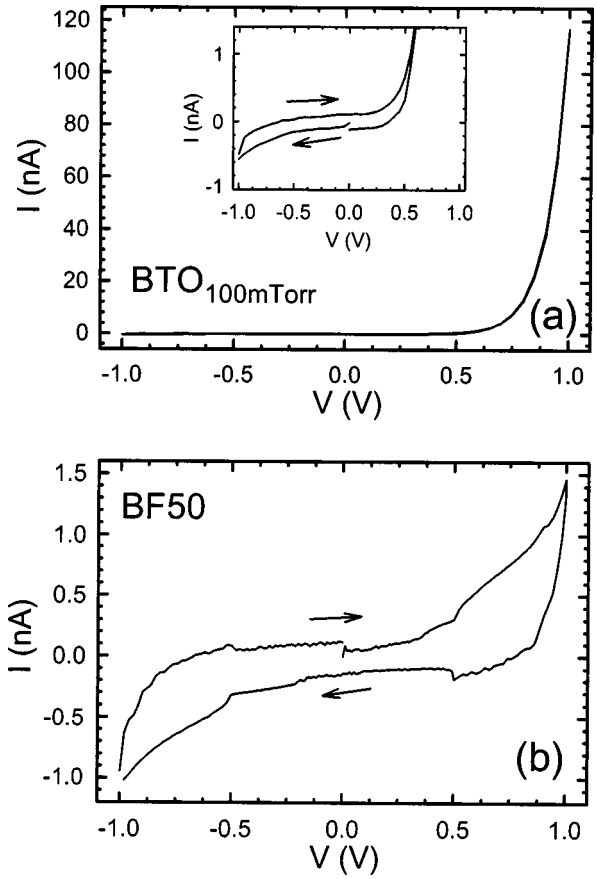

FIG. 4. $I-V$ for a 360 nm $BTO_{100mTorr}$ capacitor and a 360 nm BF50 capacitor. The inset in (a) shows part of the plot for $BTO_{100mTorr}$ in expanded scale.

(high-field) dielectric constant above T_C increases the barrier height and, hence, the resistivity. The observed resistivity upturn, although not as sharp as in bulk ceramics, is thus a strong indication that the films remain ferroelectric upon the addition of Fe. Supporting this interpretation, the $\rho_{\|}$ minimum of BF50 coincides[1] with the structural transition of the same sample shown in Fig. 2(a). The cause for the several peaks, observed in several pieces of $BTO_{100mTorr}$, is unclear at present.

Upon cooling and *subsequent* heating, the PTCR effect is absent; possibly after heating above T_C the films remain in the paraelectric phase. In $BTO_{0.12mTorr}$, $\rho_{\|}$ increases to the same level as in $BTO_{100mTorr}$ at high temperatures and remains close to $\rho_{\|}$ of $BTO_{100mTorr}$ upon cooling. It is likely that oxidation above 600 °C eliminates most oxygen vacancies. The drop of resistivity upon cooling below ~70 °C in most samples could be the signature of another phase transition, possibly related to the orthorhombic phase known in bulk BTO.[30]

The addition of iron to thin-film BTO leads to decreased resistivity and enhanced PTCR effect in BFTO. The former is likely brought about by the formation of oxygen vacancies; the latter may be associated with an increase in low-angle grain boundaries inferred from the broadening of XRD peaks.

$I-V$ at room temperature is shown in Fig. 4 for two capacitors made from BTO_{100} and BF50, respectively. The sign of the voltage is defined with respect to the top electrode. Both samples show diodelike characteristics and hysteresis resulting from competition between relaxation and leakage currents.[31]

In the case of BTO [Fig. 4(a)], reverse bias is at negative voltage which suggests the presence of a barrier at the metal electrode. The STON contact shows ohmic behavior suggesting *n*-type conduction in the BTO films; this is in agreement with previous reports.[31] In BF50 [Fig. 4(b)] the currents have equal order of magnitude at both polarities and are considerably lower than at forward bias in $BTO_{100mTorr}$ [Fig. 4(a)]. Apparently, a barrier exists at the BF50–STON junction, suggesting that BTO becomes a *p*-type semiconductor with 50% Fe substitution for Ti. Acceptor states added by Fe^{3+} are likely responsible.[26] Since leakage currents are much lower than in BTO, relaxation-type hysteresis is more pronounced. In films with more than 50% Fe, the behavior was similar to that of BF50.

Conduction through the film–metal junction appears to be dominated by Schottky emission in the presence of an insulating interfacial layer.[32] Barrier heights at the Cr–Au top electrode and effective Richardson constants were obtained from a procedure described by Dietz *et al.*[15,33] The effective Richardson constant A^* is significantly decreased as iron is added. This suggests that the oxide layer at the interface is significantly thicker for BFTO as compared to BTO. This is further supported by the asymmetry observed in capacitance-voltage measurements for BFTO.[15] Possible mechanisms through which iron could enhance an interfacial oxide layer include increased surface roughness as a consequence of the decreased crystalline quality in BFTO and increased chemical reactivity of the surface.

B. Polarization and capacitance

Polarization versus voltage measurements, performed with a Sawyer–Tower circuit, did not yield any evidence for ferroelectric hysteresis for the *a*-oriented films. This was expected, because in *a*-oriented films, the axis of polarization is in the film plane. In the *c*-oriented $BTO_{0.12mTorr}$ films, the high conductivity did not permit reliable Sawyer–Tower measurements.

Capacitance versus temperature ($C-T$) measured at 10 kHz and 100 kHz, is shown in Figs. 5(a) and 5(b) for a $BTO_{100mTorr}$ capacitor and a BF50 capacitor. Overall C is lower in BF50 than in $BTO_{100mTorr}$ and even further decreased in samples with more than 50% Fe.[15] The loss tangent in $BTO_{100mTorr}$ and BF75 is between 0.1 and 0.01 at room temperature,[15] whereas it is one order of magnitude higher in BF50; for applications values or equal to less than 0.01 would be desirable.

The temperature evolution of the capacitance shows a distinct step for BF50 just above 200 °C, at about the same temperature where anomalies were seen in the temperature dependence of lattice parameters and resistivity for this composition (Figs. 2 and 3, respectively). Apparently this step is the signature of T_C, reminiscent of the Curie–Weiss behavior of the permittivity above the ferroelectric–paraelectric phase transition for bulk materials. In the $BTO_{100mTorr}$ heat-

Downloaded 26 Sep 2007 to 129.171.61.70. Redistribution subject to AIP license or copyright, see http://jap.aip.org/jap/copyright.jsp

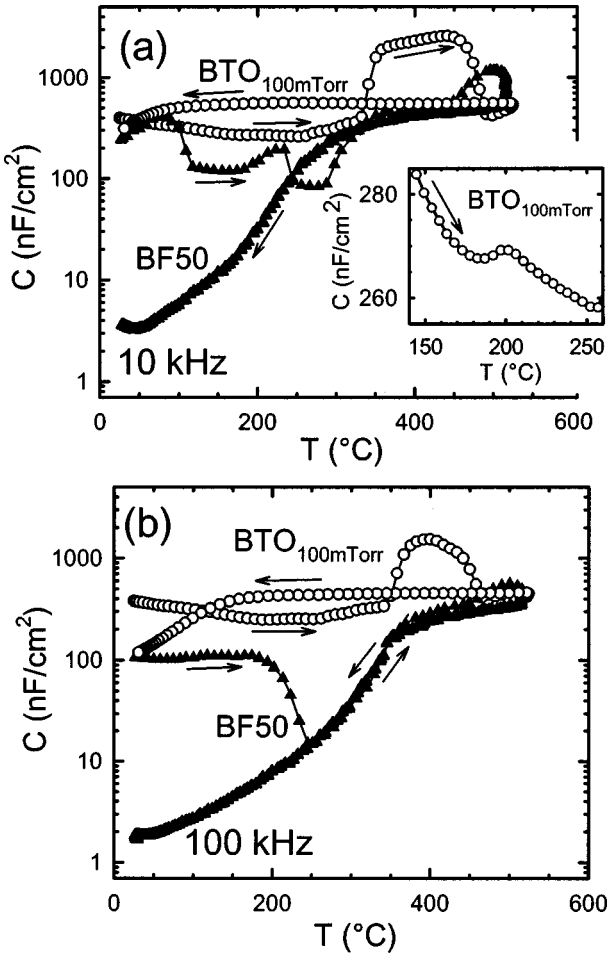

FIG. 5. $C-T$ for a 360 nm $BTO_{100mTorr}$ capacitor and a 360 nm BF50 capacitor, (a) at 10 kHz, and (b) at 100 kHz. The arrows denote heating and cooling. The inset shows the range around 200 °C for $BTO_{100mTorr}$ in linear scale.

ing curves only a broad, shallow valley is distinguishable below 300 °C in a logarithmic scale. However, in linear scale, a small peak can be distinguished [Fig. 5(a), inset] in the region between 200 °C and 230 °C, and a plot of the dielectric relaxation time versus temperature[15] shows a distinct step in that temperature region. This feature coincides with the first minimum of the resistivity. The anomalies described here are present both at 10 kHz and 100 kHz in the same temperature region. The rise of the capacitance for both specimens at $T>300$ °C is attributed to space-charge relaxation.[15,34]

Upon cooling, the capacitance for all BFTO samples[15] decreases continuously to values at room temperature that are lower by more than an order of magnitude compared to those in the as-prepared state. For $BTO_{100mTorr}$, the difference in the as-prepared and annealed capacitance at room temperature is substantially smaller. Note that this larger thermal hysteresis for BFTO was also evident in the lattice constants (Fig. 2). In consecutive $C-T$ runs, heating curves coincided with the cooling behavior. This ties in with the absence of PTCR upon cooling and consecutive heating, further supporting the hypothesis that the films remain in the paraelectric state after being heated once above T_C.

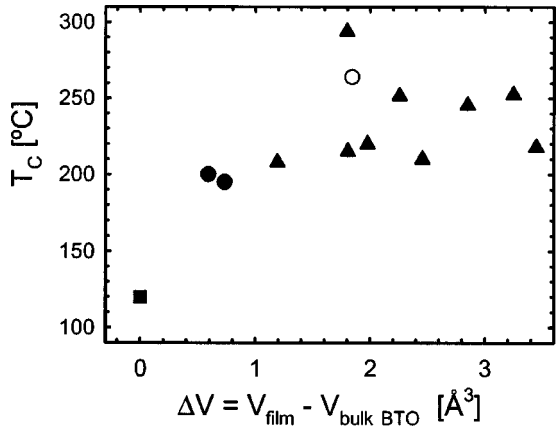

FIG. 6. T_C vs difference in film volume from that of bulk BTO. The symbols represent: Bulk BTO (closed square), $BTO_{100mTorr}$ (closed circles), $BTO_{0.12mTorr}$ (open circle), and BFTO (solid triangles).

Overall, the capacitance data are consistent with the lattice constants and resistivity, exhibiting anomalies indicative of a phase transition at and above 200 °C upon heating, but not upon cooling. The anomalies are more distinct in BFTO than in BTO. The dielectric constant is decreased by Fe doping.

C. Discussion of the paraelectric–ferroelectric phase transition

The T_C values for all films determined from lattice constants, resistivity, and/or capacitance data, correlate with unit-cell volume. In Fig. 6, we plot T_C versus the difference (ΔV) between the unit-cell volume of films and that of bulk BTO. All T_C values are considerably higher than that of bulk BTO ($T_C=120$ °C). Pertsev *et al.*[21] have demonstrated that T_C elevation is to be expected in thin-film BTO on a cubic substrate in the presence of both compressive and tensile in-plane strain. Presumably, this explains why the lowest T_C value observed for our films is ~200 °C (for $BTO_{100mTorr}$). Among the thin-film samples, there is a trend toward further T_C elevation with increasing volume. This trend is consistent with the decrease of T_C in bulk BTO under hydrostatic pressure.[35]

The phase transition is not as abrupt as in bulk BTO, as indicated by the finite temperature interval over which the transitions in lattice parameters, $\rho(T)$, and $C(f,T)$ take place. A broadening of the permittivity peak of BTO films in the presence of homogeneous strain is expected theoretically.[36] Inhomogeneous strain and crystal defects can also contribute to broadened ferroelectric–paraelectric transitions.[37] Strain inhomogeneity is usually present in films, since structural relaxation proceeds with increasing distance from the substrate.

In the BTO films, the phase transition is only indicated in resistivity and capacitance, but not in the lattice parameters. This suggests that here the ferroelectric–paraelectric phase transition occurs while at the same time the tetragonal–cubic transition is suppressed, a phenomenon reported previously.[38] Possibly, the transition is less suppressed in BFTO because its poorer crystalline quality entails a more relaxed state.

Downloaded 26 Sep 2007 to 129.171.61.70. Redistribution subject to AIP license or copyright, see http://jap.aip.org/jap/copyright.jsp

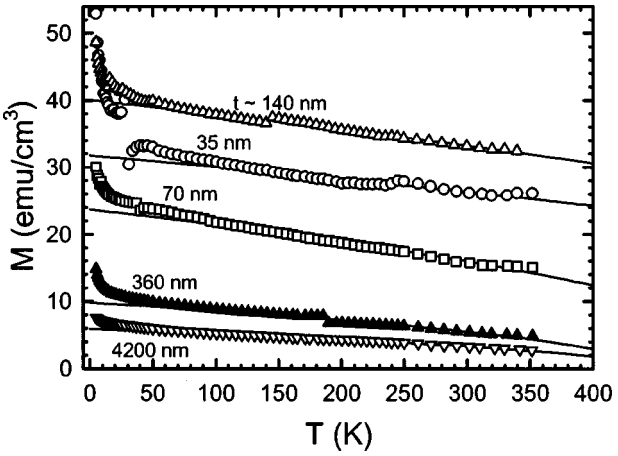

FIG. 7. $M-T$ for five BFTE samples of different thickness deposited on [100]MgO; the applied field was $H=5$ kOe in the film plane along the [100] crystallographic axis. The solid curves are fits to the mean field expression used to estimate M_{sat}.

Upon cooling, the signatures of the phase transition both in the structural and electrical data are absent in all samples. Absence of the structural signatures of the ferroelectric–paraelectric phase transition upon cooling has been previously reported for BTO films made under oxygen deficient conditions.[37] The apparent metastability of the as-prepared films might be due to the fairly fast cooling rate after deposition. Possibly, more dislocations form during the phase transition upon heating so the films are more relaxed in the paraelectric state, leading to a more stable state after cooling.

In summary, the films show a paraelectric–ferroelectric phase transition upon heating, which is suppressed upon cooling. In BTO, the structural transition is also suppressed upon heating. Due to strain, the transition is less abrupt in the films than it is in bulk BTO. T_C is raised to ~200 °C due to strain, and even more in BFTO and $BTO_{0.12mTorr}$ due to lattice expansion induced by oxygen vacancies. Thus, Fe has a two-fold effect on the ferroelectric–paraelectric phase transition: Enhancement of the transition and increase of T_C. Further studies would be necessary to clarify the cause for the modification or suppression of the phase transition upon cooling.

V. MAGNETIC PROPERTIES

Recently, we reported that BFTO films exhibit saturation behavior and hysteresis, characteristics for magnetic ordering.[1] Here, we investigate the dependence of the magnetic properties on iron content and thickness.

Magnetization versus temperature ($M-T$) is shown in Fig. 7, measured at magnetic field $H=5$ kOe in the film plane along the [100] crystallographic axis for five BFTE samples of varying thickness on [100]MgO. Similar curves were found for films grown from other BFTO targets. Disregarding the upturns below 100 K, the qualitative behavior can be described by the mean-field expression $M-T=M_{sat}(1-T/T_N)^{1/2}$, where M_{sat} is the saturation magnetization and T_N the temperature of the magnetic–paramagnetic phase transition. The mean-field fits and their extrapolations to low temperatures are indicated by the solid curves in Fig. 7. T_N, estimated from extrapolations of the fits to higher temperatures (not shown in Fig. 7), likely exceeds 450 °C for all measured samples.

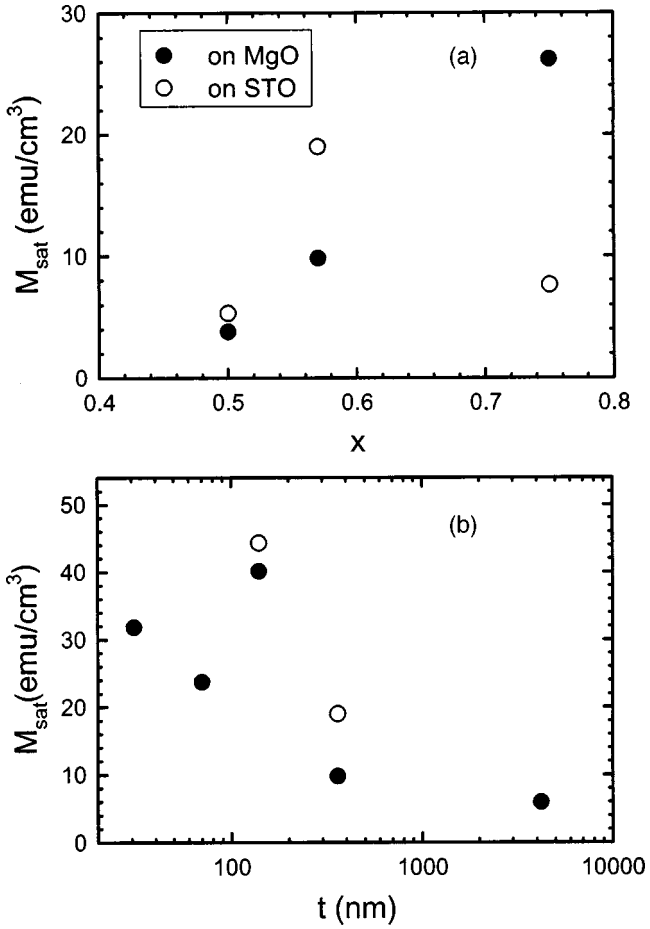

FIG. 8. M_{sat} vs Fe content [(a)] and thickness [(b)] for ~360 nm thick BFTO films.

The low-temperature upturns in the magnetization curves are attributed to target chunks at the film surface, which are typical in PLD-grown films. Three observations support this interpretation: First, the measured magnetizations of the BF50 and BF75 targets have strong paramagnetic components with roughly inverse temperature dependence. Second, by comparing the film and target magnetizations, we computed the volume of target chunks required to reproduce the upturn observed in the films. In all cases, this volume was less than or equal to the volumes of the film. Third, the upturn is largest for the thinnest films, where the volume of target chunks is expected to be a larger fraction of the film volume. We can not entirely rule out the possibility that the films themselves contain paramagnetic regions, for instance, where the local iron concentration is lowest.

M_{sat} shows two trends. First, for a given film thickness, the magnetization tends to increase with Fe content [Fig. 8(a)]. Second, for given Fe content the magnetization tends to be lower at thicknesses exceeding 140 nm [Fig. 8(b)]. Overall, the average M_{sat} of samples with thicknesses of 140 nm or less is 47.5 emu cm^{-3}, the average of all samples is 28.5 emu cm^{-3}. This trend is attributed to the disordered

Downloaded 26 Sep 2007 to 129.171.61.70. Redistribution subject to AIP license or copyright, see http://jap.aip.org/jap/copyright.jsp

phase (possibly nonmagnetic) growing atop the pseudocubic phase as the film thickness exceeds 140 nm.

For a model of the magnetic ordering in the BFTO films, consider an approximately cubic magnetic unit cell consisting of eight lattice unit cells. The average magnetization component in field direction of such a cell is given by

$$\overline{M_z} = \frac{g \times \overline{\Delta S} \times \mu_B}{8 \times V_{f.u.}},$$

where $\overline{\Delta S}$ is the average excess spin in the field direction, μ_B is the Bohr magneton; the Landé g-factor is taken to be $g=2$, the volume of a lattice unit cell (formula unit) is set to $V_{f.u.}=66$ Å^3, corresponding to an average lattice parameter of ~4.04 Å. In the following considerations, we will assume that $M_{\mathrm{fit}}(0\ \mathrm{K},5\ \mathrm{kOe})$ is a reasonable measure for the order of magnitude of the saturation magnetization, although the samples were not entirely saturated at 5 kOe. Thus, setting $\overline{M_z}=47.5\ \mathrm{emu\,cm^{-3}}$ $(\sim 0.34\ \mu_B/f.u.)$, the average $M_{\mathrm{fit}}(0\ \mathrm{K},5\ \mathrm{kOe})$ for films with $t \leqslant 140$ nm, gives $\overline{\Delta S}=1.36$. In case of ferromagnetism, the theoretical lower bound for the average excess spin is $\overline{\Delta S}=8$, assuming $x=0.5$ and Fe^{4+} $(S=2)$ only. Hence, the magnetic ordering is likely ferrimagnetic in the BFTO films.

As a guide to the exchange interactions relevant for BFTO, it is useful to examine the closest relative for which magnetism has been reported, $BaFeO_x$ $(x \sim 2.5-2.95)$.[39–45] Most of these reports refer to a hexagonal phase of $BaFeO_x$; only Mori[40] studied the pseudocubic phase as well. Mori[40] reports that the $Fe^{4+}-Fe^{4+}$ interaction is ferromagnetic, while the $Fe^{3+}-Fe^{3+}$ and $Fe^{3+}-Fe^{4+}$ interactions are antiferromagnetic. This suggests that the BFTO samples contain a significant fraction of both Fe^{4+} and Fe^{3+}. Assuming equal concentrations of Fe^{3+} and Fe^{4+} for simplicity, and ferrimagnetism with all Fe^{3+} and Fe^{4+} spins antialigned, a theoretical average excess spin of $\overline{\Delta S}=1$ per magnetic unit cell is obtained. This is close to the value 1.36 inferred from the average M_{sat}.

In conclusion, the substitution of 50% or more of titanium by iron in thin-film pseudocubic BTO leads to ferrimagnetic ordering. The ferrimagnetic–paramagnetic transition temperature T_N likely exceeds 450 °C. The saturation magnetization is estimated as $\sim 50\ \mathrm{emu\,cm^{-3}}$ in the thinner films, and is 10%–20% lower at room temperature. The coercive and remanent fields of all samples measured are reported elsewhere.[15]

VI. SUMMARY

Thin-film $BaFe_xTi_{1-x}O_3$ with $0 \leqslant x \leqslant 0.75$ was grown epitaxially by PLD on MgO, STO, and STON. The structure of the main phase is pseudocubic tetragonal (orthorhombic). The orientation of the pseudocubic unit cells is mainly determined by the oxygen pressure during deposition; high pressure resulted in *a* orientation, low pressure in *c* orientation. The crystalline quality in *a*-oriented BTO films is among the best reported for thin-film BTO. The replacement of 50% or more of Ti by Fe deteriorates the crystalline quality, leads to ferrimagnetic ordering well above room temperature, and converts BTO from an *n*-type to a *p*-type semiconductor. The ferroelectric–paraelectric phase transition in BTO and BFTO films is greatly modified as compared to bulk BTO. Strain imposed by the substrate raises T_C to ~200 °C; introduction of oxygen vacancies, either via the lowering of P_{O_2} during deposition or by Fe doping, causes further T_C elevation. The transition is broadened, mainly as a consequence of strain, and absent upon cooling and subsequent heating. In BTO, the *structural* phase transition is suppressed even upon first heating.

In its present form, $BaFe_xTi_{1-x}O_3$ exhibits losses too high for microwave applications and a resistivity too low to serve as a good dielectric. However, BFTO does have technological potential because of the simultaneous electric and magnetic ordering. Interesting physics is also displayed in the suppression of the ferroelectric–paraelectric phase transition upon cooling.

A better understanding is yet required to judge if further development could improve BFTO sufficiently to make it useful, e.g., for microwave applications or as a ferroelectromagnet. Further investigation could focus on clarifying the oxidation state of Fe via Mössbauer measurements, and on determining if interactions between electrical and magnetical ordering can indeed be exploited for useful applications.

ACKNOWLEDGMENTS

The authors acknowledge Professor J. J. Neumeier for providing PLD targets, materials characterization, and fruitful discussions. Also acknowledged are discussions with Professor N. Pertsev, Dr. L. Rotter, and Professor C. Vittoria, and experimental assistance from D. Kukuruznyak and S. Schuler. This work was supported, in part, by NSF Grant Nos. DMR-9504213 and DMR-0072276.

[1] R. Maier, J. L. Cohn, J. J. Neumeier, and L. A. Bendersky, Appl. Phys. Lett. **78**, 2536 (2001).
[2] R. Kullmer, Appl. Phys. A: Mater. Sci. Process. **65**, 273 (1997).
[3] B. H. Hoermann, G. M. Ford, L. D. Kaufmann, and B. W. Wessels, Appl. Phys. Lett. **73**, 2248 (1998).
[4] M. H. Frey and D. A. Payne, Appl. Phys. Lett. **63**, 2753 (1993).
[5] T. Nose, H.-T. Kim, and H. Uwe, Jpn. J. Appl. Phys., Part 1 **33**, 5259 (1994).
[6] Y. Yoneda, K. Sakaue, and H. Terauchi, Jpn. J. Appl. Phys., Part 1 **39**, 4839 (2000).
[7] L. A. Bendersky, R. Maier, J. L. Cohn, and J. J. Neumeier, J. Mater. Res. **15**, 1389 (2000).
[8] T. A. Vanderah, J. M. Loezos, and R. S. Roth, J. Solid State Chem. **121**, 38 (1996).
[9] R. Maier, J. L. Cohn, J. J. Neumeier, and L. A. Bendersky, *Magnetoresistive and Related Oxides*, edited by M. Rzchowski, M. Kawasaki, A. J. Millis, M. Rajeswari, and S. von Molnár, (Materials Research Society, Pittsburgh), Conference Vol. 602.
[10] S. Kim, S. Hishita, Y. M. Kang, and S. Baik, J. Appl. Phys. **78**, 5604 (1995).
[11] F. Jona and G. Shirane, *Ferroelectric Crystals* (Pergamon, New York, 1962), p. 108.
[12] D.-Y. Kim, S.-G. Lee, Y.-K. Park, and S. J. Park, Jpn. J. Appl. Phys., Part 2 **34**, L1564 (1995).
[13] M. Hiratani, K. Imagawa, and K. Takagi, Jpn. J. Appl. Phys., Part 1 **34**, 254 (1995).
[14] R. W. G. Wyckoff, *Crystal Structures* (Interscience, New York, 1960), Vol. 2.
[15] R. Maier, Doctoral dissertation, 2002.
[16] K. P. Fahey, B. M. Clemens, and L. A. Wills, Appl. Phys. Lett. **67**, 2480 (1995).

Downloaded 26 Sep 2007 to 129.171.61.70. Redistribution subject to AIP license or copyright, see http://jap.aip.org/jap/copyright.jsp

[17] E. J. Tarsa, E. A. Hachfeld, F. T. Quinlan, J. S. Speck, and M. Eddy, Appl. Phys. Lett. **68**, 490 (1996).
[18] W. J. Kim, W. Chang, S. B. Qadri, J. M. Pond, S. W. Kirchoefer, D. B. Chrisey, and J. S. Horwitz, Appl. Phys. Lett. **76**, 1185 (2000).
[19] H.-J. Hagemann, A. Hero, and U. Gonser, Phys. Status Solidi A **61**, 63 (1980).
[20] R. D. Shannon, Acta Crystallogr., Sect. A: Cryst. Phys., Diffr., Theor. Gen. Crystallogr. **32**, 751 (1976).
[21] N. A. Pertsev, A. G. Zembilgotov, and A. K. Tagantsev, Phys. Rev. Lett. **80**, 1988 (1998).
[22] Y. S. Touloukian, R. K. Kirby, R. E. Taylor, and T. Y. R. Lee, *Thermophysical Properties of Matter* (Plenum, New York, 1977), Vol. 13.
[23] J. Zhang, D. Cui, Y. Zhou, L. Li, M. Szabadi, and P. Hess, Thin Solid Films **287**, 101 (1996).
[24] N.-Y. Lee, T. Sekine, Y. Ito, and K. Uchino, Jpn. J. Appl. Phys., Part 1 **33**, 1484 (1994).
[25] T. Hioki, H. Funakubo, O. Sakurai, K. Shinozaki, and N. Mizutani, J. Ceram. Soc. Jpn. **104**, 75 (1996).
[26] M. B. Klein, *Photorefractive Materials and Their Applications*, edited by P. Günther and J. P. Huignard (Springer, Berlin, 1988), Vol. 61, p. 195.
[27] W. Heywang, Solid-State Electron. **3**, 51 (1961).
[28] G. H. Jonker, Solid-State Electron. **7**, 895 (1964).
[29] G. V. Lewis, C. R. A. Catlow, and R. E. W. Casselton, J. Am. Ceram. Soc. **68**, 555 (1985).
[30] T. Zhao, Z.-H. Chen, F. Chen, H.-B. Lu, G.-Z. Yang, and H.-S. Cheng, Appl. Phys. Lett. **77**, 4338 (2000).
[31] M. Okano, D. Sawamura, and Y. Watanabe, Jpn. J. Appl. Phys., Part 1 **37**, 5101 (1998).
[32] S. M. Sze, *Physics of Semiconductor Devices* (Wiley, New York, 1981).
[33] G. W. Dietz, M. Schumacher, R. Waser, S. K. Streiffer, C. Basceri, and A. I. Kingon, J. Appl. Phys. **82**, 2359 (1997).
[34] O. Bidault, P. Goux, M. Kchikech, M. Belkaoumi, and M. Maglione, Phys. Rev. B **49**, 7868 (1994).
[35] G. A. Samara, Phys. Rev. **151**, 378 (1966).
[36] N. A. Pertsev, A. G. Zembilgotov, S. Hoffmann, R. Waser, and A. K. Tagantsev, J. Appl. Phys. **85**, 1698 (1999).
[37] C. Li, Z. Chen, D. Cui, Y. Zhou, H. Lu, C. Dong, F. Wu, and H. Chen, J. Appl. Phys. **86**, 4555 (1999).
[38] Y. Yoneda, H. Kasatani, H. Terauchi, Y. Yano, T. Terashima, and Y. Bando, J. Phys. Soc. Jpn. **62**, 1840 (1993).
[39] H. Kobayashi, F. Iga, and Y. Nishihara, Nucl. Instrum. Methods Phys. Res. B **76**, 258 (1993).
[40] S. Mori, J. Phys. Soc. Jpn. **28**, 44 (1970).
[41] J. B. MacChesney, J. F. Potter, R. C. Sherwood, and H. J. Williams, J. Chem. Phys. **43**, 3317 (1965).
[42] P. K. Gallagher, J. B. MacChesney, and D. N. E. Buchanan, J. Chem. Phys. **43**, 516 (1965).
[43] F. Iga, Y. Nishihara, G. Kido, and Y. Takeda, J. Magn. Magn. Mater. **104**, 1969 (1992).
[44] F. Iga, Y. Nishihara, T. Katayama, K. Murata, and Y. Takeda, J. Magn. Magn. Mater. **104**, 1973 (1992).
[45] S. Mori, J. Am. Ceram. Soc. **49**, 600 (1966).

Downloaded 26 Sep 2007 to 129.171.61.70. Redistribution subject to AIP license or copyright, see http://jap.aip.org/jap/copyright.jsp